



HAL
open science

Guidelines for data-driven approaches to study transitions in multiscale systems: The case of Lyapunov vectors

Akim Viennet, Nikki Vercauteren, Maximilian Engel, Davide Faranda

► **To cite this version:**

Akim Viennet, Nikki Vercauteren, Maximilian Engel, Davide Faranda. Guidelines for data-driven approaches to study transitions in multiscale systems: The case of Lyapunov vectors. *Chaos: An Interdisciplinary Journal of Nonlinear Science*, 2022, 32, pp.113145. <10.1063/5.0093804>. <hal-03626146v2>

HAL Id: hal-03626146

<https://hal.science/hal-03626146v2>

Submitted on 14 Nov 2022

HAL is a multi-disciplinary open access archive for the deposit and dissemination of scientific research documents, whether they are published or not. The documents may come from teaching and research institutions in France or abroad, or from public or private research centers.

L'archive ouverte pluridisciplinaire **HAL**, est destinée au dépôt et à la diffusion de documents scientifiques de niveau recherche, publiés ou non, émanant des établissements d'enseignement et de recherche français ou étrangers, des laboratoires publics ou privés.



HAL Authorization

1 **Guidelines for data-driven approaches to study transitions in multiscale systems: the**
2 **case of Lyapunov vectors**

3 Akim Viennet,^{1, a)} Nikki Vercauteren,^{2, b)} Maximilian Engel,^{3, c)} and Davide Faranda^{4, d)}

4 ¹⁾*Department of Physics, Ecole Normale Supérieure, 75005 Paris,*
5 *France*

6 ²⁾*Department of Geosciences, University of Oslo, 0371 Oslo,*
7 *Norway*

8 ³⁾*Institute of Mathematics, Freie Universität, 14195 Berlin,*
9 *Germany*

10 ⁴⁾*Laboratoire des Sciences du Climat et de l'Environnement,*
11 *UMR 8212 CEA-CNRS-UVSQ, Université Paris-Saclay, IPSL,*
12 *91191 Gif-sur-Yvette, France*

13 (Dated: 14 November 2022)

14 We study in detail the role of covariant Lyapunov vectors and their respective an-
15 gles for detecting transitions between metastable states in dynamical systems, as
16 recently discussed in several atmospheric science applications. The underlying mod-
17 els are built from data by the dynamical clustering method, called FEM-BV-VAR,
18 and the Lyapunov vectors are approximated based on these models. We test this
19 data-based numerical approach at the hand of three well-understood example sys-
20 tems with increasing dynamical complexity, identifying crucial properties that allow
21 for a successful application of the method: in particular, it turns out that the method
22 requires a clear multiple time scale structure with fast transitions between slow sub-
23 systems which can be dynamically characterized by invariant neutral directions of
24 the linear approximation model.

a) akim.viennet@gmail.com

b) nikki.vercauteren@geo.uio.no

c) maximilian.engel@fu-berlin.de

d) davide.faranda@lsce.ipsl.fr; also at London Mathematical Laboratory, 8 Margravine Gardens London, W6 8RH, UK; and also at LMD/IPSL, Ecole Normale Supérieure, PSL research University, Paris, France

25 In climate science, systems with multiple metastable states are ubiquitous. In
26 non-equilibrium systems with a non-stationary but steady forcing or intrinsic
27 noisy dynamics, metastability denotes an intermediate energetic state other than
28 the system's state of least energy: the fluctuations in the forcing parameter or
29 in the dynamics can enable the system to reach metastable states and stay there
30 for a finite amount of time, then leaving into another regime before coming back
31 with a positive probability. Knowing their stability properties and the probability
32 of transitioning from one state to another is of great help to understand and pre-
33 dict the dynamics of such systems. Many tools have been developed to address
34 this challenge, among which covariant Lyapunov vectors have proven to be very
35 useful. The numerical calculation of these vectors generally requires an a priori
36 knowledge of the set of equations governing the dynamics, and therefore cannot
37 be applied directly to experimental data. However, recent purely data-driven
38 methods have been developed to estimate the covariant Lyapunov vectors. Our
39 study aims to identify the crucial conditions under which a data-driven factor
40 model approach can successfully estimate the alignment of covariant Lyapunov
41 vectors to predict critical transitions. To this end, we discuss in detail the FEM-
42 BV-VAR approach for multiscale systems and test the method on three systems
43 of increasing dynamic complexity, including two explicit classical models and
44 experimental data for turbulent flow. As the tested method is expected to be
45 relevant in a wide range of climate science applications, our key contribution is
46 to show under which circumstances reliable results can be expected.

47 I. INTRODUCTION

48 Dynamical systems theory deals with the prediction of trajectories of natural systems
49 originating by one given or a set of initial conditions. This task is particularly challenging
50 when the system is chaotic and even more when the system features several metastable
51 states or multiscale features^{1,2}. Among all the possibilities, here we focus on the stability
52 properties of certain meta-stable states, that organize the phase space, and the estimation
53 of the probability of switching from one state to another. Many mathematical tools have

54 been developed to address those questions, one of them being the study of the so-called
55 *covariant Lyapunov vectors* (CLVs) (also known as Oseledets vectors), and the associated
56 *Lyapunov exponents* (LEs). These vectors give a basis on the tangent space at points of
57 trajectories, providing directions of linear perturbation growth along the dynamics³⁻⁵. They
58 can be seen as a generalization of the linear stability theory for fixed points and of Floquet's
59 theory for limit cycles, since Lyapunov vectors and exponents can be computed along any
60 trajectory of a smooth dynamical system. The CLVs give the directions of growth or decay
61 of a perturbation, and the LEs give the associated rate of asymptotic growth or decay. An
62 increase of one of the unstable LEs has been associated to a higher instability for various
63 theoretical and physical systems^{6,7}.

64 In many cases, transient (chaotic) behavior cannot be detected by asymptotic LEs which
65 average out transient dynamics via ergodic limits; hence, *finite-time Lyapunov exponents*
66 (FTLEs) are often more suitable to capture the degree of uncertainty at different points of
67 trajectories and their small neighbourhoods.

68 The directions of unstable CLVs indicate the directions towards which an error will grow
69 with the rates given by the associated (FT)LEs. For example, this tool can be used in
70 ensemble weather forecasting to identify how to enforce initial perturbations to optimally
71 span the space of possible realizations of the weather⁸. Another quantity of interest is the
72 angle between the flow direction and the most unstable CLV. An alignment of those vectors
73 has been used as a predictor for transitions, tipping points or catastrophes (extreme events)
74 in several systems⁹⁻¹¹. In particular, this criterion has been proven to be an important early-
75 warning sign for abrupt transitions in the Peña and Kalnay climate toy-model¹². Finally,
76 Quinn et al.¹³ suggested that the projection of the most unstable CLV just before a transition
77 between two states could inform on the patterns that triggered the instability and then the
78 transition.

79 Summarizing, the computation of CLVs and associated LEs is of high interest for the
80 analysis of dynamical systems. Recent progress was made to compute them numerically,
81 due to various algorithms by Ginelli et al.⁴, Wolfe and Samelson⁵, and Froyland et al.¹⁴.
82 However, all those algorithms rely on the knowledge of an analytic expression of the model,
83 in order to differentiate the flow and compute the linear cocycles (see Section II B for an
84 introduction to those methods). This suggests that it is rather difficult to use such methods
85 based on observations for which the underlying model is unknown or only partially known,

86 such as reanalysis atmospheric data.

87 Yet, recent progress has been made to estimate CLVs from data series. Lately, Martin
88 et al.¹⁵ suggested to use sparse identification of non-linear dynamics to infer the Jacobian
89 matrices from trajectories. Quinn et al.¹³ recently introduced another method to compute
90 CLVs directly from data, aimed at dealing with systems with stochastic transitions. This
91 latter method will be studied and tested in this paper. It relies on fitting a model to
92 the observations via a dynamical, or model-based clustering method initially introduced by
93 Horenko^{16,17}: the FEM-BV-VAR (Finite Element clustering with bounded variation (FEM
94 BV) vector autoregressive (VAR)) clustering approach. Differently from more classical,
95 geometrical clustering methods, in this framework a state is not defined by a geometrical
96 area in the phase space, but by an estimated auto-regressive dynamics (see Section III A
97 for details). The whole system is then switching between those dynamical models. This
98 method is particularly adapted to the purpose since it provides not only a cluster affiliation
99 sequence, but also a linear (auto-regressive) model for each of the states. One can then
100 use these (approximated) models to compute an approximation of the CLVs and of the LEs
101 for the dynamical system underlying the data, and thus get some insights on the stability
102 of the states and of the stable and unstable directions. Quinn et al.¹³ used this approach
103 to analyse the dynamics of atmospheric circulation patterns in the northern hemisphere.
104 They investigated the dynamical stability properties of recurrent and persistent states of
105 the atmospheric circulation patterns or regimes known as the North Atlantic Oscillation
106 (NAO) and atmospheric blocking events. In particular, the CLVs were used to analyse
107 the pressure distribution patterns related to transitions between the recurrent circulation
108 regimes, leading to insightful observations since weather forecasting and climate models
109 struggle to capture the onset and decay of blocking events.

110 These results led to the question whether the method is applicable for other systems of
111 interest and to which extent it more generally captures relevant information on the dynam-
112 ics. The aim of this work is to explore this question by testing the method in several systems
113 for which some a priori knowledge of the CLVs and of the transitions between regimes is
114 available: a fast-slow FitzHugh-Nagumo oscillator, a well-studied Von Kármán turbulent
115 flow from a laboratory experiment, and a Lorenz 63 system, where the order of our presen-
116 tation follows an increase of dynamical complexity. Results on those different systems will
117 show that the method provides several insights on the dynamics, quantifying the stability of

118 different (meta-stable) states and thereby identifying transitions between them. This holds
119 true in particular for the Von Kármán flow. However, we also demonstrate why such con-
120 clusions may be treated with caution, considering the strong dependence on the existence of
121 an dynamically invariant normal tangent flow direction, a visible time scale separation and
122 a large number of hyper-parameters.

123 In this paper, we will first present the details of the method that allows one to compute
124 approximated CLVs from a data series. Then we will try to assess its validity, by applying
125 it on a FitzHugh-Nagumo oscillator, experimental data from the Von Kármán flow and the
126 Lorenz 63 model. Finally, we will discuss the scope of the methods at the hand of these
127 examples, illustrating its potential but also several caveats for its application.

128 **II. THE LYAPUNOV VECTORS AND THEIR NUMERICAL** 129 **COMPUTATION**

130 **A. Mathematical background**

131 Let us first introduce the notion of CLVs. They arise from a non-autonomous general-
132 ization of the linear stability analysis at fixed points and Floquet theory at limit cycles to
133 any point of the trajectory. For a dynamical system, the CLVs form a basis of the tangent
134 space and give the directions of growth or decay of any perturbation around a background
135 flow. The Lyapunov exponents (LEs) give the associated rate of growth or decay (see Fig.1).
136 Assuming ergodicity of a dynamical system $\Phi_t(x_0)$, whose trajectories we will simply denote
137 by $x(t)$, one observes that the LEs are global numbers that characterise the whole attrac-
138 tor, whereas the CLVs may depend on the particular points of the trajectory (but are still
139 asymptotic objects).

In more detail, the existence of Lyapunov exponents with corresponding directions on
the tangent space is given by Oseledets' Multiplicative Ergodic Theorem (MET)¹⁸. Under
a mild integrability condition with respect to an ergodic invariant measure, this theorem
gives us, in each point of the trajectory, the existence of a splitting of the tangent space into
 $p \leq d$ subspaces

$$\mathbb{R}^d = Y_1(x(t)) \oplus \cdots \oplus Y_p(x(t)),$$

140 such that for all $v \in Y_i(x(t))$,

$$\lim_{\tau \rightarrow \infty} \frac{1}{\tau} \log \|\mathcal{F}(t, t + \tau) \cdot v\| = \lambda_i, \quad (1)$$

where \mathcal{F} denotes the linear propagator for the tangent flow, i.e.

$$v(t_2) = \mathcal{F}(t_1, t_2) v(t_1)$$

141 and $\lambda_1 > \lambda_2 > \dots > \lambda_p$ are the distinct LEs with multiplicities $m_i \geq 1$, $i = 1, \dots, p$. The
 142 CLVs $v_i^j(t)$, $j = 1, \dots, m_i$, are then representative vectors from the Oseledets subspaces
 143 $Y_i(x(t))$, which are unique up to scalar factors if $m_i = 1$ and chosen as a set of m_i linearly
 144 independent vectors in $Y_i(x(t))$ otherwise. Let us order them as ϕ_k , $k = 1, \dots, d$, where
 145 $v_1^1 = \phi_1, \dots, v_1^{m_1} = \phi_{m_1}$, and so on (see also Figure 1 where all $m_i = 1$ as will be the case in
 146 our examples).

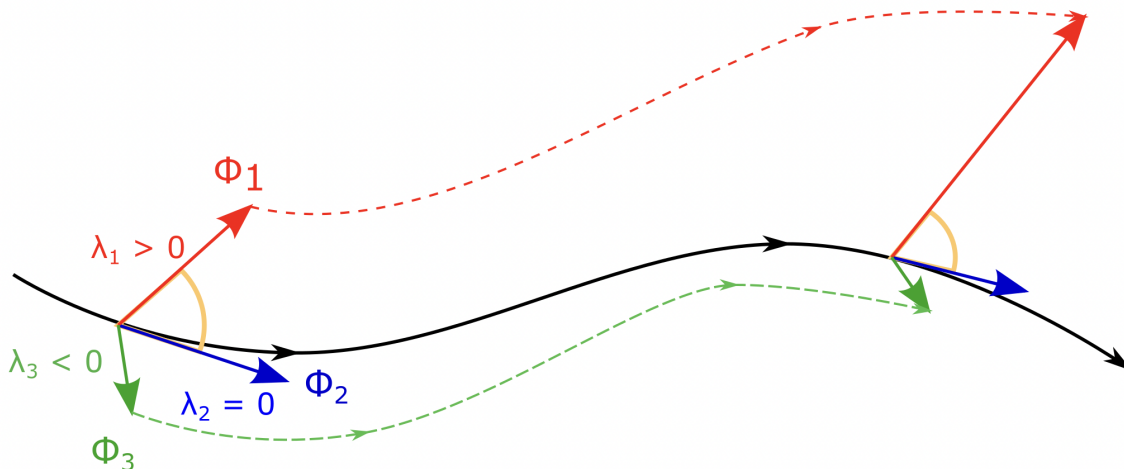


FIG. 1: Contraction and expansion of CLVs along a trajectory with positive, negative and zero Lyapunov exponent λ_i , $i = 1, 2, 3$. In this setting, we have at each point three CLVs (ϕ_1 , ϕ_2 and ϕ_3). The solid line represents the unperturbed trajectory, while the dotted lines represent the perturbed trajectories, along the stable (in green) and the unstable (in red) directions. The so-called alignment θ_{12} is given by the cosine of the orange angle.

147

148

149 As described in Section I, LEs and CLVs give important information on the stability
 150 properties of the dynamics, and have been used to predict transitions and extreme events.
 151 One key quantity is the angle between the neutral CLV (the CLV associated with a zero LE,

152 which is always tangent to the flow direction) and the most unstable CLV (the one associated
 153 with the largest positive LE), given that they both exist. Let us call θ_{ij} the cosine of the
 154 angle between the CLVs ϕ_i and ϕ_j :

$$\theta_{ij}(t) = \frac{|\phi_i(t) \cdot \phi_j(t)|}{\|\phi_i(t)\| \|\phi_j(t)\|} \quad (2)$$

155 Many studies suggest that, for ϕ_i representing the most unstable direction and ϕ_j a neutral
 156 direction, this angle is related to the probability of transitions between characteristic states:
 157 the more these two vectors align, the higher such a switching probability is expected to
 158 be. Sharafi et al.⁹ have applied this criterion to various fast-slow systems, whereas Beims
 159 et al.¹⁰ have used it to predict extreme events in a Rössler oscillator. In the following, we
 160 will call “alignment of CLVs” the absolute value of the cosine of the angle between a most
 161 unstable CLV and a neutral one. In cases without a neutral direction, one may take the
 162 CLV associated with the Lyapunov exponent closest to 0 and consider this direction as a
 163 *near-neutral* one (see also Section IV C).

164 Note that the CLVs and associated Lyapunov exponents are asymptotic objects whereas
 165 the transitions we are interested in happen on finite time scales and the analyzed time series
 166 are also naturally finite. Hence, in reality one analyzes *Finite Time Lyapunov Exponents*
 167 (FTLEs) which are defined analogously for a given finite τ in Eq.(1), depending on space and
 168 time. FTLEs associated to CLVs (or their finite time approximations one may also regard to
 169 as Finite Time Lyapunov vectors (FTLVs)) may change their signs depending on τ . In some
 170 cases, there can exist strictly positive FTLEs even though the trajectory is asymptotically
 171 stable (i.e. all LEs are negative). This is typical for globally asymptotically stable systems
 172 with transient chaos. In particular, an asymptotically stable (or unstable) CLV might be
 173 referred to as an unstable (or stable) CLV on certain finite time scales. Hence, we will call
 174 CLVs stable or unstable in our numerical studies based on the local stability within the
 175 investigated finite time scales. The FitzHugh-Nagumo oscillator discussed below exemplifies
 176 this: while the trajectories asymptotically approach a stable periodic orbit (one negative,
 177 one neutral LE), the CLVs and associated FTLEs can detect the local instability along the
 178 fast subsystem (see Section IV A for further explanations). Generally speaking, FTLEs can
 179 be used as a measure for the predictability of the local dynamics: the higher the largest
 180 FTLE, the lower the predictability on the respective time scale (see, for example, Deremble

181 et al.¹⁹ for the classical Lorenz 63 attractor and a one-layer quasi-geostrophic atmospheric
 182 model). As suggested by Quinn et al.¹³ (and before by Deremble et al.¹⁹), the time length
 183 τ acts as a scale filter for the dynamics: with small τ the computed FTLEs and the related
 184 CLVs (or FTLVs) give insights on the short scale processes, whereas with larger τ we get
 185 closer and closer to asymptotic properties.

186 B. Direct computation of the CLVs

187 There exist several algorithms to numerically compute the CLVs. One of the most famous
 188 methods was developed in 2007 by Ginelli et al.⁴. However, here we will use a modified
 189 approach introduced in 2013 by Froyland et al.¹⁴ (algorithm 2.2 in this reference). This
 190 choice is motivated empirically by a faster convergence and by more consistent results in the
 191 considered setting, when compared to results obtained with Ginelli’s algorithm.

The *Froyland algorithm* relies on a singular value decomposition of the forward cocycles starting at past fibers, then propagating the obtained orthogonal directions into covariant ones. Thus, computing the CLVs at a given point on the trajectory requires a pullback procedure from the past to the present (and beyond). This involves a number of time steps N for going to the past and a number of time steps M corresponding with the time length τ in Eq. (1). In this study, for simplicity we always take $M = N$ (as suggested in Froyland’s article and validated empirically). In theory, increasing N and M improves the approximation. However, our results show that convergence may fail due to the accumulation of numerical errors. Therefore, N and M are key parameters that act as a scale filter, similarly to τ in the previous subsection. Another internal parameter to be adapted is given by the number of correction steps n for obtaining the covariant out of singular directions; for details see algorithm 2.2 in Froyland et al.¹⁴. To sum up, this algorithm requires to set three parameters:

$$M, N \text{ and } n$$

192 with, in this study, $N = M$.

193 Finally, let us emphasise that this algorithm requires an explicit expression for the lin-
 194 ear propagator at each point. For continuous-time systems $\dot{x} = f(t, x)$, the linear prop-
 195 agator solves the variational linear differential equation with matrix generator $J(x, t) :=$
 196 $(D_x f)(t, x)$, i.e. the Jacobian of the vector field f . For discrete-time systems $x_{n+1} = g(x_n)$,

197 the propagator is the product of the matrices $A_n = (D_x g)(x_n)$. Hence, computing the quan-
 198 tities directly from data, for which the propagator is not known a priori, is out of reach.
 199 The aim of this article is to investigate the capabilities of the above-mentioned Froyland’s
 200 algorithm for computing approximate CLVs directly from observed time series, relying on
 201 a prior modelling step using a model-based clustering framework. We hence explore, based
 202 on systems of different complexity, the conditions under which the method first introduced
 203 in¹³ provides reliable results.

204 III. DYNAMICAL CLUSTERING METHOD

205 A. FEM-BV-VAR approach

206 In the literature, various approaches address the problem of identifying persistent states
 207 based on data. They can be roughly classified as either *non-dynamical* or *dynamical* meth-
 208 ods. The class of non-dynamical methods only exploits geometrical properties of the data for
 209 clustering, regardless of their temporal occurrence. The most used non-dynamical approach
 210 is the k-means method, which clusters data points according to their minimal distance to ge-
 211 ometrical centroids of point clouds²⁰. Dynamical methods additionally take into account the
 212 temporal changes of data, based on latent variables models such as hidden Markov models²¹.
 213 This work considers a dynamical clustering method in which the existence of multiple states
 214 is presumed, each having time-independent properties. Those states are presumed to have
 215 a certain degree of persistence, and the system transitions between them during its evo-
 216 lution. A simplified description of the dynamics is then given in terms of a set of locally
 217 stationary linear vector autoregressive models (the cluster states). This method is coined
 218 as FEM-BV-VAR approach (Finite Element clustering with bounded variation (FEM BV)
 219 Vector autoregressive (VAR))^{16,17}. Due to its proven utility in modeling transitional behav-
 220 ior between persistent meta-stable states directly from data, FEM-BV-VAR has recently
 221 become popular to study dynamical aspects of the atmosphere, ocean, and climate systems;
 222 studies have tackled small-scale processes in the atmospheric boundary layer^{22,23}, as well
 223 as large-scale atmospheric and oceanic circulation^{13,24,25}. Importantly, the method does not
 224 rely on any underlying assumptions regarding the statistical stationarity of the data and,
 225 hence, is applicable to problems where trends are present.

226 In the FEM-BV-VAR approach, a cluster is defined as a subset of the observed time
 227 series of data whose evolution can be described approximately by a stationary linear vector
 228 autoregressive model. The full time series is modeled as a set of such stationary VAR models,
 229 with a switching process representing transitions between the cluster states. Since the states
 230 are assumed to have a certain degree of persistence, the dynamical evolution of the system is
 231 described by VAR models describing the fast-scale dynamics within a given state, while the
 232 slow evolution is described by the switching process. Hence, the dynamics is decomposed
 233 into two parts:

- 234 • a locally stationary fast auto-regressive (VAR) process,
- 235 • a slow hidden process that makes the system switch between different forms of such
 236 auto-regressive processes (i.e. between the different states).

237 Within a given state, we assume the time evolution of the vector of observables \mathbf{x}_t to be
 238 governed by

$$\mathbf{x}_t = \mu^{(i)} + \sum_{\tau=1}^m \mathbf{A}_\tau^{(i)} \mathbf{x}_{t-\tau} + \epsilon_t^{(i)} \quad (3)$$

where $\mu^{(i)}$ is the mean of the i -th cluster, $\mathbf{A}_\tau^{(i)}$ are matrices, and $\epsilon_t^{(i)}$ is a white noise with a
 covariance matrix $\Sigma^{(i)}$. A state of the system (or cluster) i is then characterized by its set
 of parameters

$$\Theta_i = \left(\mu^{(i)}, \mathbf{A}_1^{(i)}, \dots, \mathbf{A}_m^{(i)}, \Sigma^{(i)} \right).$$

239 A set of K such models is assumed, with different model coefficients in (3), leading to K
 240 clusters. Determination of the optimal coefficients in (3) is done via minimization based on
 241 the distance between the observations and the deterministic part of the model

$$g(\mathbf{x}_t, \theta(t)) = \left\| \mathbf{x}_t - \mu^{(i)}(t) - \sum_{\tau=1}^m \mathbf{A}_\tau^{(i)}(t) \mathbf{x}_{t-\tau} \right\|, \quad (4)$$

242 calculated for a fixed temporal realisation of parameters $\theta(t)$. The functional to minimize
 243 also includes a cluster affiliation term that determines the set of model parameters the data
 244 should be associated with and is then given as

$$L(\Theta, \Gamma(t)) = \sum_{t=0}^T \sum_{i=1}^K \gamma_i(t) g(\mathbf{x}_t, \Theta_i), \quad (5)$$

245 where Θ denotes the collection of all Θ_i , i.e. $\Theta = (\Theta_1, \dots, \Theta_K)$ and T the time length of
 246 the observed dynamics. The functions $\Gamma(t) = (\gamma_1(t), \dots, \gamma_K(t))$ are the cluster affiliation

247 functions whose values give the probability of the data at time t to belong to cluster i and
 248 should satisfy the following property at a given time t

$$\sum_{i=1}^K \gamma_i = 1, \quad \gamma_i \geq 0 \quad \forall i = 1, \dots, K \quad (6)$$

249 The number K and the memory depth m are hyper-parameters that must be selected.
 250 The assumption of local stationarity of the statistical process is finally enforced by setting a
 251 persistence parameter C , which defines the maximum allowed number of transitions between
 252 a total of K different statistical processes. This step regularises the minimization problem
 253 by introducing the additional constraint on the total variation norm of the sequence

$$\sum_{t=0}^{T-1} |\gamma_i(t+1) - \gamma_i(t)| \leq C, \quad \forall i = 1, \dots, K. \quad (7)$$

254 This last hyper-parameter C is also more conveniently defined via the average persistence p
 255 as $C = \frac{T}{p} - 1$. The reader is referred to Horenko¹⁶ and references therein for further details
 256 about the method and the minimization process.

257 This method makes it possible to detect dynamical patterns that would not be detected
 258 by a geometrical method such as the k-means: for instance, a change in frequency of the
 259 signal or some oscillations with multiple amplitudes. It also provides a local linear model
 260 for the data, on which the computation of the Covariant Lyapunov Vectors will be based.
 261 However, it is important to bear in mind that three hyper-parameters (K, m, p) have to be
 262 selected when fitting a model.

263 B. Choosing the hyper-parameters

264 Statistical techniques based on information theory were developed to find the best hyper-
 265 parameters of the FEM-BV-VAR (namely the number of clusters K , the memory depth m
 266 and the average persistence p)^{16,17}. Here, physical understanding of the systems is also used
 267 to choose K and m , as will be detailed when presenting the results. The persistence p is
 268 selected via the so called L-curve method: as shown by Horenko¹⁶, the optimal value of p can
 269 be determined as the edge point (or the point of maximal curvature) on a two- dimensional
 270 plot, where one plots the total distance between the model and the data against the value
 271 of p . In the application of the FEM-BV-VAR algorithm, the reconstructed signal has been
 272 found to diverge in some configurations; hence, we have checked the output of the algorithm

273 manually and sometimes slightly modified p around its optimal value if the model, indeed,
 274 diverges (results not shown).

275 C. Data-driven computation of the CLVs through the FEM-BV-VAR

276 The direct computation of CLVs requires an analytical expression of the linearized dy-
 277 namics (in order to apply Froyland’s algorithms to the linear propagator). Hence, such a
 278 computation is not feasible via purely data-driven approaches. The idea introduced by¹³ is
 279 to use the auto-regressive linear model obtained by the FEM-BV-VAR clustering step as an
 280 underlying model to describe the dynamical system. Let us recall that the FEM-BV-VAR
 281 gives us a VAR model for each of the K states

$$\mathbf{x}_t = \mu^{(i)}(t) + \sum_{\tau=1}^m \mathbf{A}_\tau^{(i)}(t) \mathbf{x}_{t-\tau} + \epsilon_t^{(i)}$$

From this we deduce a discrete linear dynamical system (here given for $m = 3$) :

$$\begin{bmatrix} \mathbf{x}_{t+1} \\ \mathbf{x}_t \\ \mathbf{x}_{t-1} \end{bmatrix} = \begin{bmatrix} \mathbf{A}_1^{(i_{t+1})} & \mathbf{A}_2^{(i_{t+1})} & \mathbf{A}_3^{(i_{t+1})} \\ \mathbf{I} & \mathbf{0} & \mathbf{0} \\ \mathbf{0} & \mathbf{I} & \mathbf{0} \end{bmatrix} \begin{bmatrix} \mathbf{x}_t \\ \mathbf{x}_{t-1} \\ \mathbf{x}_{t-2} \end{bmatrix}$$

where i_{t+1} is the index of the state of the system at time $t + 1$. We can therefore compute the cocycle $\mathcal{F}(t, t + \tau) = \mathcal{A}(t + \tau) \dots \mathcal{A}(t)$, with

$$\mathcal{A}(t) = \begin{bmatrix} \mathbf{A}_1^{(i_{t+1})} & \mathbf{A}_2^{(i_{t+1})} & \mathbf{A}_3^{(i_{t+1})} \\ \mathbf{I} & \mathbf{0} & \mathbf{0} \\ \mathbf{0} & \mathbf{I} & \mathbf{0} \end{bmatrix}$$

282 Using the described approach, Quinn et al.¹³ analyzed the dynamics of the North Atlantic
 283 Oscillation, using daily means of the 500 hPa geopotential height as input data. The cluster-
 284 ing framework was used to characterise the persistent states in the atmospheric circulation,
 285 and the uncovered model was used to analyse the dynamical properties of different regimes.
 286 In particular, a finite-time dimension measure for the linear dynamical system was used to
 287 characterize the instability of each regime, thereby identifying the largest dimension to be
 288 associated with a given state of the NAO, namely the blocked state. They also considered
 289 the most unstable CLVs just before a transition from one state to another, to investigate

290 which atmospheric pattern was driving the instability. The results appeared consistent with
291 previous studies based on different methodologies. This raised the following question: to
292 what extent are the CLVs, computed in such a manner, significant dynamic indicators and
293 can this method be applied to a large class of systems? In the following, we will test thor-
294 oughly this method on systems for which many dynamical aspects are known: a fast-slow
295 FitzHugh-Nagumo oscillator, a well-studied Von Kármán turbulent flow from a laboratory
296 experiment, and a Lorenz 63 system.

297 IV. OBSERVATIONS AND GUIDELINES

298 The purpose of the study is to determine the conditions under which the results obtained
299 by computing the CLVs of a data series through the FEM-BV-VAR model are reliable. The
300 method is applied to systems for which a priori knowledge of the states and of their stability
301 exists. In terms of dynamical structure, the examples are introduced following an increase
302 in complexity: the method is first applied on a fast-slow FitzHugh-Nagumo oscillator with
303 two distinct time scales, then on data extracted from a laboratory experiment of a flow
304 whose dynamics highlight a periodic orbit and a saddle point. Finally, the chaotic Lorenz
305 attractor, which presents the most complex dynamics, is investigated.

306 Our main finding is that this procedure works well provided the studied system exhibits
307 two properties (which are related to each other). Firstly, it should have a clear scale sepa-
308 ration in time, that is, one should be able to distinguish a time scale gap between two (or
309 more) phenomena in the dynamics, as, for instance, in standard fast-slow systems. Scale
310 separation can be estimated in several different ways, depending on the availability of data
311 and on the existence of differential equations to describe the dynamics^{26–29}. Secondly, the
312 system needs a (near-)neutral direction along trajectories which is invariant under the lin-
313 ear(ized) dynamics: indeed, if the system does not have any neutral direction, the angle
314 θ is no longer a relevant quantity to evaluate the stability of a state. This condition is
315 frequently satisfied in physical systems, exhibiting invariant center manifolds where the hy-
316 perbolic dynamics take place; these are exactly the *slow manifolds* in the fast-slow situation.
317 For the data-driven approach to be successful, this neutral direction has to be preserved by
318 the FEM-BV-VAR reconstructed model. This is a crucial challenge as we will see in the
319 following.

320 **A. The case of a fast-slow FitzHugh-Nagumo oscillator**

As described in Section III A, the FEM-BV-VAR method is developed to study systems with a certain fast-slow structure, detecting the transition between states that are characterized by their respective fast dynamics. Therefore, the method is well-suited for models with time scale separation, expressed by a parameter $0 < \epsilon \ll 1$, that exhibit switches between different branches of the slow manifold consisting of equilibria of the fast subsystem. A by now canonical example of such a fast-slow system is the FitzHugh-Nagumo ODE (8) (see also Figure 2), which was derived as a simplification of the Hodgkin-Huxley model for an electric potential of a nerve axon³⁰:

$$\begin{aligned}\epsilon \frac{dx}{d\tau} &= \epsilon \dot{x} = x - \frac{x^3}{3} - y, \\ \frac{dy}{d\tau} &= \dot{y} = x + a - by.\end{aligned}\tag{8}$$

Note that by a time change $t = \tau/\epsilon$, we may also write

$$\begin{aligned}\frac{dx}{dt} &= x' = x - \frac{x^3}{3} - y, \\ \frac{dy}{dt} &= y' = \epsilon(x + a - by).\end{aligned}\tag{9}$$

321 Setting $\epsilon = 0$ in equation (9), one can study the *fast subsystem* for which y is a bifurcation
 322 parameter and whose y -dependent set of equilibria is given by the curve $y = x - x^3/3$,
 323 also called *critical manifold* S_0 . The cubic nonlinearity entails a bistable structure with
 324 two fold points that mark a change of stability of the fast subsystem. Considering one of
 325 the two (hyperbolically) stable branches of S_0 , one may also take $\epsilon = 0$ in equation (8)
 326 and observe how the *slow subsystem* evolves along S_0 . This gives a normal (or neutral)
 327 y -direction together with a hyperbolic x -direction, yielding, for $\epsilon > 0$, two branches of a
 328 *slow manifold* S_ϵ around the stable branches of S_0 with the same stability properties³¹. At
 329 the mentioned fold points this *normal hyperbolicity* breaks down and fast switches occur
 330 between the two branches of the slow manifold (in accordance with the coloring in Figure 2
 331 (a).) The described behavior is also called *relaxation-oscillation*, famously associated with
 332 the van der Pol oscillator as a paradigm model, for which the FitzHugh-Nagumo ODE is a
 333 slight generalization³². Summarizing, Figure 2 shows transitions between a left and a right
 334 branch of a slow manifold. Along each of these branches, there is an actual neutral direction
 335 complemented by a stable one for most of the time until both directions (almost) coincide
 336 into a locally unstable direction around the fold (or transition) points. Hence, the alignment
 337

338 variable θ_{12} , where the stability of the CLVs is associated with the respective FTLEs, is an
 339 appropriate observable for detecting such transitions, see also Figure 2 (b).

340 In Figure 2, the CLVs are computed via the FEM-BV-VAR clustering method: a FEM-
 341 BV-VAR auto-regressive model is first fitted to the timeseries of observations (x, y) (see
 342 Section III A), for which the best hyper-parameters are found to be $K = 2$ (number of
 343 clusters), $m = 1$ (memory depth) and $p = 175$ (persistence), with an integration step
 344 $\tau = 0.003$. In this example, the choice of K , m and p is straightforward: the system has
 345 two well identifiable states, leading to $K = 2$, and the averaged persistence can easily be
 346 estimated by measuring the time spent by the system in each branch, leading to the estimate
 347 for p . Then, the result is fairly robust to variations in m , such that the simplest value $m = 1$
 348 is selected for the analysis. Having obtained an explicit linear model purely from the time
 349 series, the CLVs are approximated using the SVD-based algorithm (see Section II B), taking
 350 $N = M = 10$ and $n = 3$. The CLV directions are robust under higher choices of N , M and
 351 n . Note that the sign of the associated FTLEs depends on these choices; however, since
 352 we are interested in manifesting the transition behavior happening on short time scales, the
 353 small choices of N , M , n are suitable. The alignment θ_{12} follows precisely the same profile

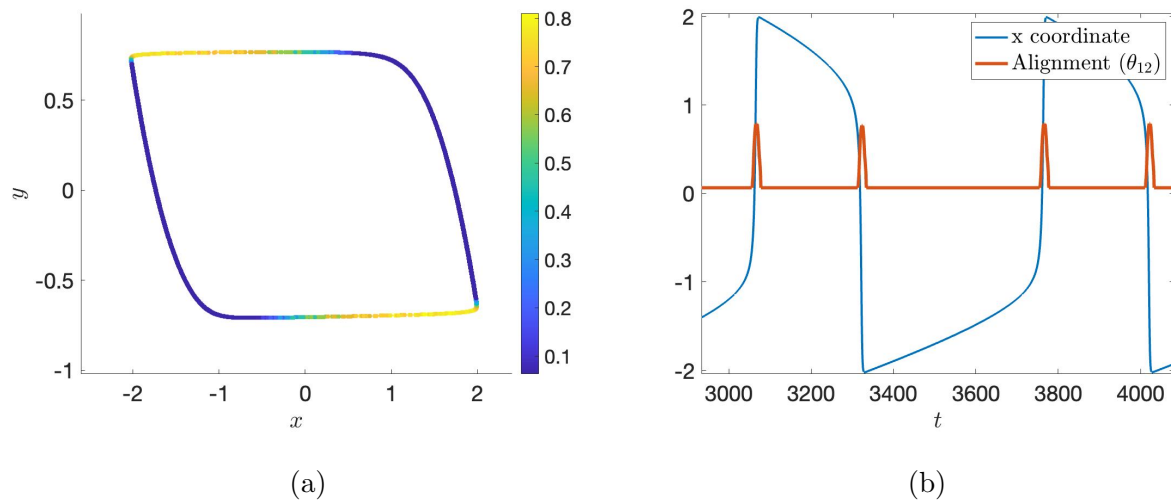


FIG. 2: (a) Trajectory in the $x - y$ plane of the FitzHugh-Nagumo system, colored according to the alignment θ_{12} , taking $\epsilon = 0.01$, $a = 0.4$, $b = 0.3$ (standard choices, as in Sharafi et al.⁹). Yellow areas correspond to unstable CLVs being close to the neutral direction. (b) Time series of the x coordinate (blue) and of the alignment θ_{12} (red).

354 as the one obtained through a direct computation of the CLVs from the linearization of the
 355 explicit FitzHugh-Nagumo ODE (8). Sharafi et al.⁹ also obtained a very similar pattern
 356 when they studied the CLVs of the FitzHugh-Nagumo system, based on another algorithmic
 357 procedure. Thus, the data-based method is successful for this example: via a pattern for
 358 θ_{12} , one can clearly identify transitions between metastable states (corresponding with slow
 359 manifolds) through the most (finite time) unstable CLV direction (corresponding with the
 360 fast one).

361 The results confirm the hypothesis that systems with a clear time scale separation and
 362 a slow manifold with an actual neutral mode are well-suited for using the FEM-BV-VAR
 363 method on time series and then detecting transitions between branches of such a slow man-
 364 ifold via the observable θ_{12} .

365 B. The case of the von Kármán attractor

366 Next, the method is tested on a more complex example issued from laboratory turbulent
 367 flows. In this case, the dynamics is indeed slightly more complex than in the FitzHug-
 368 Nagumo model: as will be shown in this section, an attractor can be constructed for this
 369 flow using an embedding procedure. This embedded attractor shows a periodic orbit as well
 370 as a saddle point.

371 The experimental set-up is that of a von Kármán swirling flow, a device designed and
 372 maintained at the Service de Physique de l'état Condensé of the Commissariat de l'Energie
 373 Atomique in Saclay, France³³⁻³⁶. The von Kármán turbulent flow is generated in a vertical
 374 cylinder filled with water and stirred by two coaxial, counter-rotating impellers. Those
 375 impellers provide energy and momentum flux at the upper and lower ends of the cylinder
 376 (see Fig. 2 in Dubrulle 2022³⁶). We focus on the case where the impellers are driven by two
 377 independent motors, operating in conditions such that the torques C_1 and C_2 applied by
 378 the flow onto the top and bottom impellers are stationary. A control parameter is defined,
 379 which is capable of tracking the symmetry of the forcing, namely $\zeta = (C_1 - C_2)/(C_1 + C_2)$.
 380 To quantify the global response of the flow to the forcing, the rotating frequencies f_1 and f_2
 381 of the two impellers are measured independently. This leads to the definition of the variable
 382 $T = (f_1 - f_2)/(f_1 + f_2)$, useful to characterize the symmetries of the flow. Indeed, previous
 383 studies^{34,35} have identified a precise relationship between values of T and instantaneous

384 configuration of the flow: $T \simeq 0$ corresponds to a quasi-symmetric turbulent flow with two
385 large scale circulation cells close to the impellers, and turbulence concentrated around the
386 central section of the cylinder. For increasing $|\zeta|$, bifurcations of the flow are observed and
387 lead to positive or negative values of T . Those correspond to flow geometries where a single
388 large scale circulation structure occupies all the flow except for a turbulent boundary layer
389 located close to the upper or lower turbine, depending on the sign of T . When $|\zeta| > 0.06$,
390 the von Kármán flow spontaneously switches among symmetric and bifurcated states and
391 the dynamical switches can be approximately described by a low-dimensional attractor³⁵.

This attractor can be visualised with the embedding procedure, plotting $(T_m, T_{m+\tau}, T_{m+2\tau})$. Here we will consider the case $\tau = 500$ and we refer to Faranda et al.³⁵ for further details on the experiment and the choice of the parameters. The obtained embedded attractor is represented in Fig.3. It shows two persistent states: on the left a meta-stable periodic orbit, and on the right a saddle point. The system spends more time spinning around the periodic orbit than around the saddle point. From the experimental data, one can only be hypothetical about the number of unstable directions of the saddle node; however, it is clear that this fixed point supports at least one stable (attracting) and at least one unstable (repulsive) direction. We apply the FEM-BV-VAR clustering method (see Section III A) to the time series of T . To that end, the first step is to choose the best FEM-BV-VAR hyper-parameters, namely the number of states K , the memory depth m and the persistence p . The embedding procedure highlights the existence of two clear states, a periodic orbit and a saddle node, thus $K = 2$. Then a grid search is performed to select values for m and p . As a criterion, we select the parameters that magnify the distinction between the periodic orbit and the saddle point, which corresponds to our intuition of the system behavior. The choice is based on a visual inspection of the output of the FEM-BV-VAR. The following values are finally selected:

$$k = 2, \quad m = 1, \quad p = 90.$$

392 The corresponding state affiliation is shown in Fig. 3, where each point of the embedded
393 attractor $(T_m, T_{m+\tau}, T_{m+2\tau})$ is colored according to its affiliated FEM-BV-VAR cluster (also
394 called state). One sees that the yellow state clearly corresponds to the cycle, and the blue one
395 to the neighbourhood of the saddle point. The FEM-BV-VAR thus successfully captures the
396 dynamical states. Let us recall that beyond the state affiliation, the FEM-BV-VAR provides

397 a linear auto-regressive model to describe the local dynamics within a state.

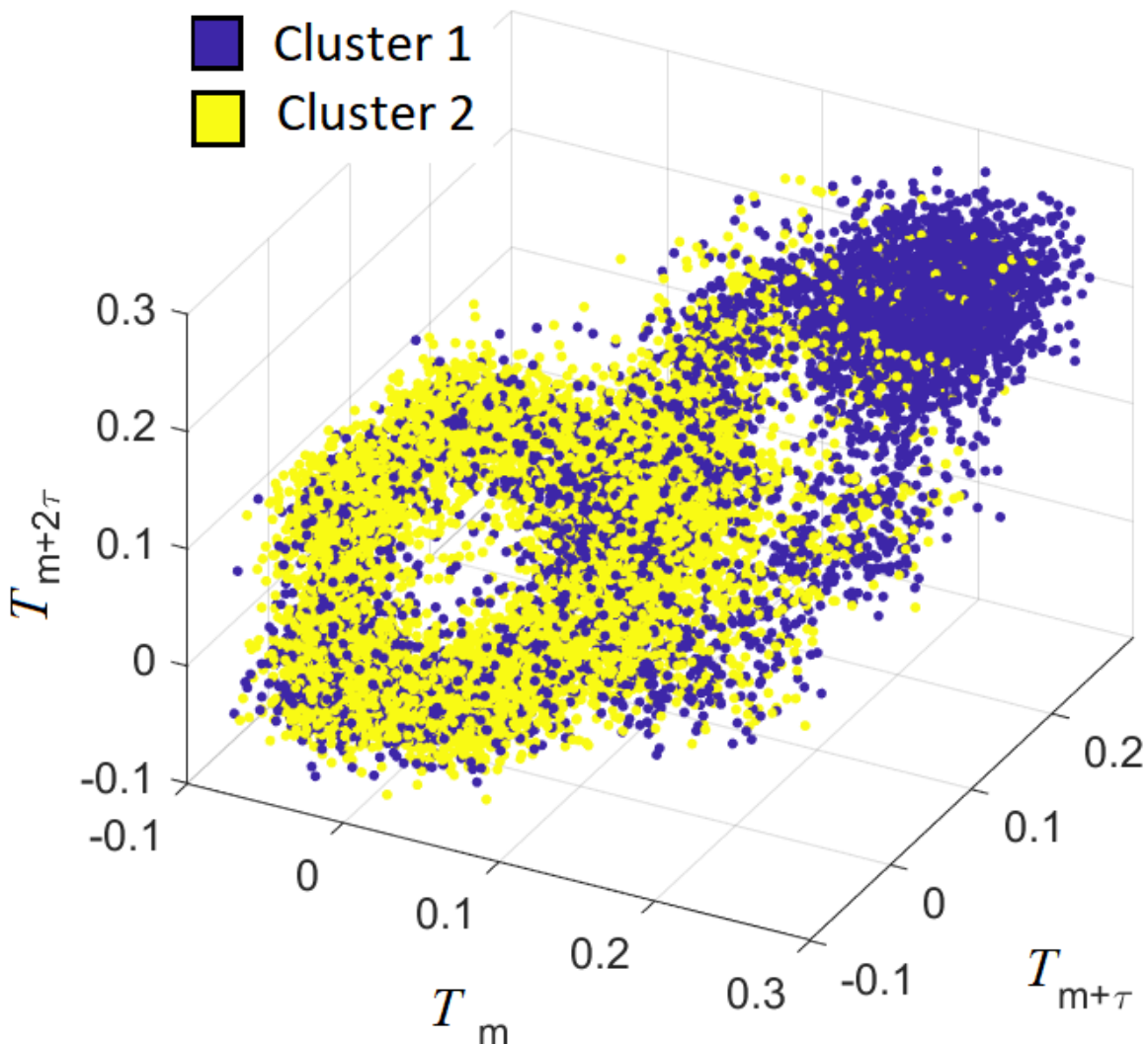


FIG. 3: FEM-BV-VAR clustering on the embedded attractor for the time series of the variable T , from the Von Kármán experimental data. Points that the algorithm detected as part of a neighbourhood of the periodic orbit are colored in yellow, and points that are associated to the saddle point, in blue. Parameters for the FEM-BV-VAR: $K = 2$, $m = 1$, $p = 90$.

398 The CLVs are then computed based on the linear model given by the FEM-BV-VAR.
399 We do not expect to have an accurate computation of the CLVs in each point, but aim at
400 estimating the relative stability of each state. Previous work^{35,36} on the von Kármán flow
401 experiment provide the results that can be expected: the periodic orbit is more strongly

402 stable than the saddle point, as it is associated with the symmetric flow (see Fig. 2 in
 403 Faranda et al.³⁵). We show that the data-driven approach to compute the CLVs can retrieve
 404 this result directly from the data, looking at the alignment θ_{12} between the most unstable
 405 CLV and the near-neutral one.

406 To that end, Froyland’s algorithm (see Section II B) is applied to the linear auto-regressive
 407 model given by the FEM-BV-VAR clustering. Three parameters need to be selected to apply
 408 the algorithm: the number of push forward steps M , the number of backward steps N and
 409 the correction step n . For simplicity we take $N = M$. A grid search is then applied on
 410 $N(= M)$ and n . For each configuration, the CLVs and the alignment θ_{12} (as defined in
 411 Eq. (2)) are computed. Fig. 4 shows the obtained result for one configuration of $N(= M)$
 412 and n , which is consistent with the expected result. The color corresponds to the value of
 413 the alignment θ_{12} , plotted on the embedded attractor, for $N = M = 30$ and $n = 1$. Around
 414 the periodic orbit the values of θ_{12} are clearly lower than around the saddle point, which
 415 means that the orbit is more strongly stable. However, the grid search (Fig. 5) shows that
 416 the result is not completely robust and depends on the choice of N and n .

417 To highlight the relative stability of the periodic orbit compared to the saddle point, the
 418 following difference is defined:

$$\Delta_{VKM} = \text{average of } \theta_{12} \text{ around the periodic orbit} - \text{average of } \theta_{12} \text{ around the saddle point} \quad (10)$$

419 Fig. 5 shows, for each choice of (N, n) , the value of the difference Δ between the average
 420 alignment θ_{12} on the orbit and around the saddle point. In most configurations, the difference
 421 is negative, that is to say the periodic orbit is more strongly stable than the saddle point
 422 (which is the expected result). However, care is needed because for some choices of (N, n)
 423 the result is precisely the opposite. Thus, N and n should be large enough, but for larger
 424 values of N , θ_{12} appears to become noisy (likely due to accumulation of numerical errors).
 425 Therefore the choice of N and n is a sensitive step, for which no systematic guidelines
 426 are available. However, the grid search used in this study supports a suitable selection of
 427 parameters, in combination with some a priori knowledge of the dynamics.

428 Nonetheless, this shows that for well suited values of the FEM-BV-VAR parameters (the
 429 number of states K , the memory depth m and the persistence p) and of Froyland’s algorithm
 430 parameters N and n , one can obtain a very insightful information on the relative stability

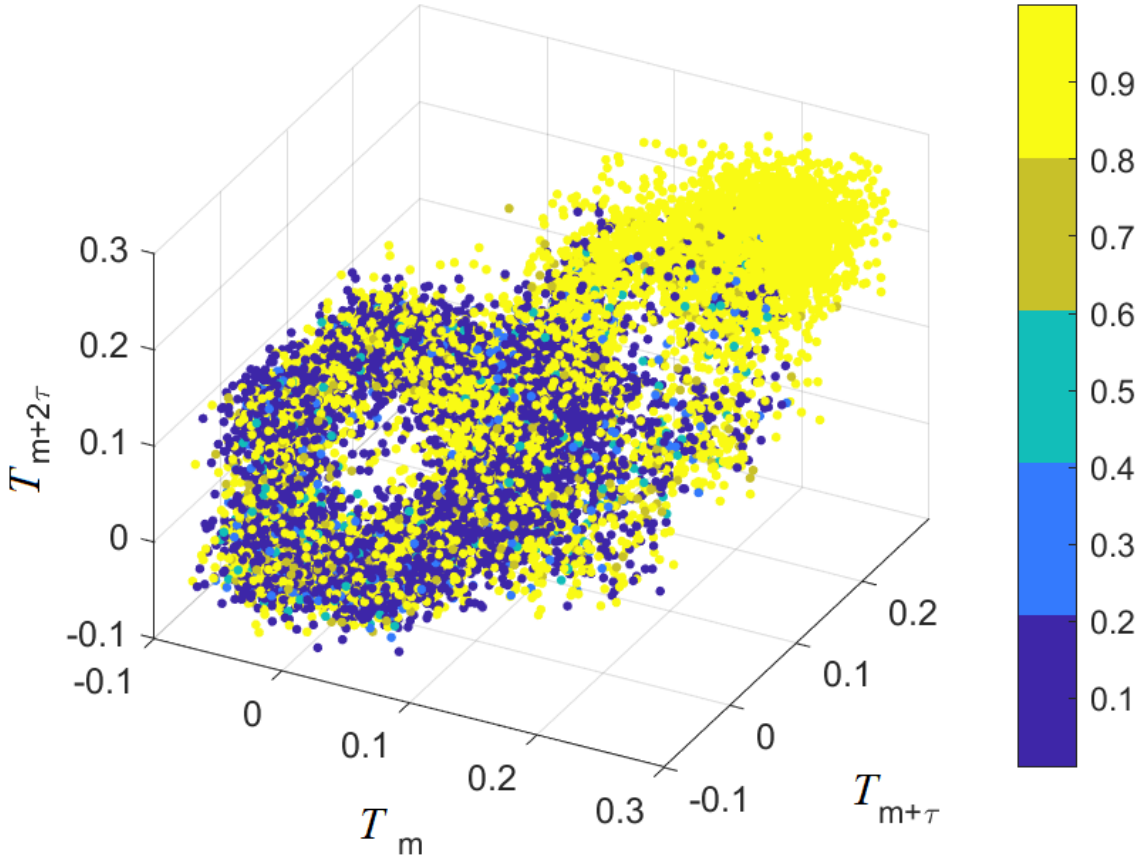


FIG. 4: CLVs alignment θ_{12} on the VKM embedded attractor. Colors correspond to the value of θ_{12} . In this configuration, the periodic orbit (in blue) appears to be more strongly stable than the saddle point (in yellow), which is the expected result. Parameters for the FEM-BV-VAR: $K = 2$, $m = 1$, $p = 80$. Parameters for Froyland's algorithm: $N = 30$, $n = 1$

431 of the states of the system, without any *a priori* information other than the raw data. This
 432 illustrates the potential validity of this method, even with experimental data. The example
 433 also supports our hypothesis that the existence of both a scale separation and a neutral
 434 direction is essential for the success of this method. In the von Kármán flow embedded
 435 attractor, one clearly has a scale separation in the sense that the trajectory oscillates for
 436 some time around one state (either the cycle or the point), and then quickly switches to
 437 the other state, with a characteristic time much faster than the oscillation. The existence
 438 of a neutral direction is more delicate to conclude, given that we do not have an underlying

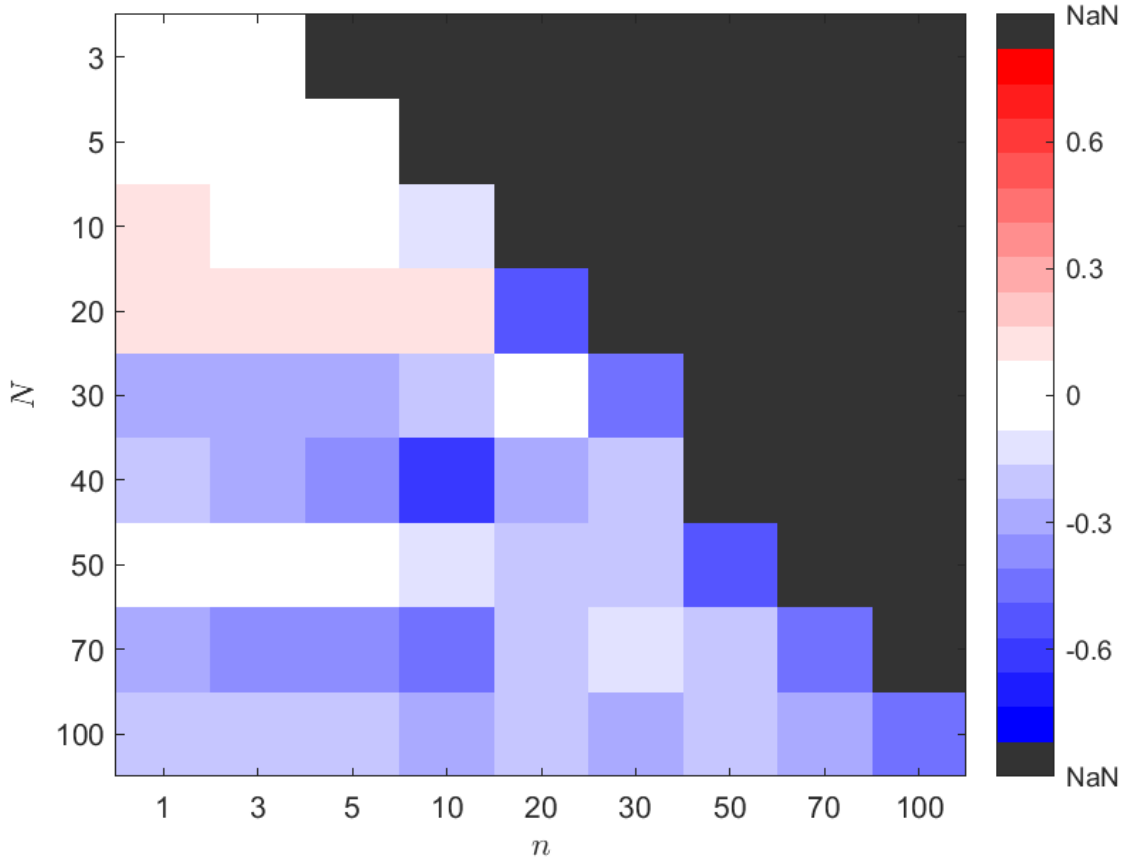


FIG. 5: Difference Δ_{VKM} between the average alignment in state 1 (periodic orbit) and 2 (saddle point), as defined in Eq. (10). N is the number of backward and forward steps (note that $M = N$), and n is the correction step (see II B). The blue areas correspond to the set of parameters for which the cycle is more strongly stable than the saddle point, which is expected.

439 analytical model. However, the existence of the anticipated neutral direction is consistent
 440 with the observed quasi-periodic motion.

441 C. On a Lorenz 63 model

442 To complete the study, the method is tested on a single Lorenz 63 system, with the usual
 443 parameters for obtaining a chaotic attractor ($\sigma = 10, \beta = 8/3, \rho = 28$)³⁷ :

$$\begin{aligned}
\frac{dx}{dt} &= \sigma(y - x), \\
\frac{dy}{dt} &= x(\rho - z) - y, \\
\frac{dz}{dt} &= xy - \beta z.
\end{aligned}
\tag{11}$$

The attractor is self-excited with respect to three equilibria: two unstable equilibria at the center of each wing and one saddle node at the origin, see Fig. 6. The system exhibits no attracting limit cycle such that the oscillations within each wing are aperiodic, exhibiting no asymptotically exact neutral direction for the linearization. The dynamics in each of the wings is sometimes described as metastable, with fast switches between them, such that one might think of a time scale separation. However, the associated patterns are highly irregular and not clearly associated to fast-slow dynamics (see also Figure 7). Dynamically speaking, this system is the most complex of this study. Regarding the Lyapunov exponents, a computation from the set of equations (11) gives (as computed through Ginelli’s procedure⁴):

$$\lambda_1 = 0.9, \lambda_2 = 0.005, \lambda_3 = -14.5.$$

444 These correspond to an unstable, a near-neutral and a stable direction respectively. Using
445 the Froyland algorithm, one can compute the CLVs along the trajectory using the analytical
446 expression of the equations (see Section II B). Fig. 6 shows the value of the alignment θ_{12}
447 (cosine of the angle between the most unstable CLV and the near-neutral one), plotted
448 onto the trajectory of the Lorenz 63 system. Blue areas correspond to low values of θ_{12} ,
449 therefore to more stable regions, and yellow areas to more unstable accordingly. Previous
450 studies showed that the alignment of CLVs computed directly from the set of equations was
451 a relevant tool to predict regime transition in the Lorenz 63 model¹¹. In this study, we aim
452 at assessing whether the FEM-BV-VAR model captures enough dynamical information for
453 the approximated data-driven CLVs to follow a similar pattern as in Fig. 6.

As for the previous examples, one has first to choose the three parameters of the FEM-BV-VAR (namely the number of states K , the memory depth m and the persistence p , see Section III A), which is harder in this example. $K = 2$ comes naturally as the attractor has two wings. As explained in Section III B, the value of the persistence p can be optimally chosen thanks to the L-curve method, provided we already fixed K and m . To choose m ,

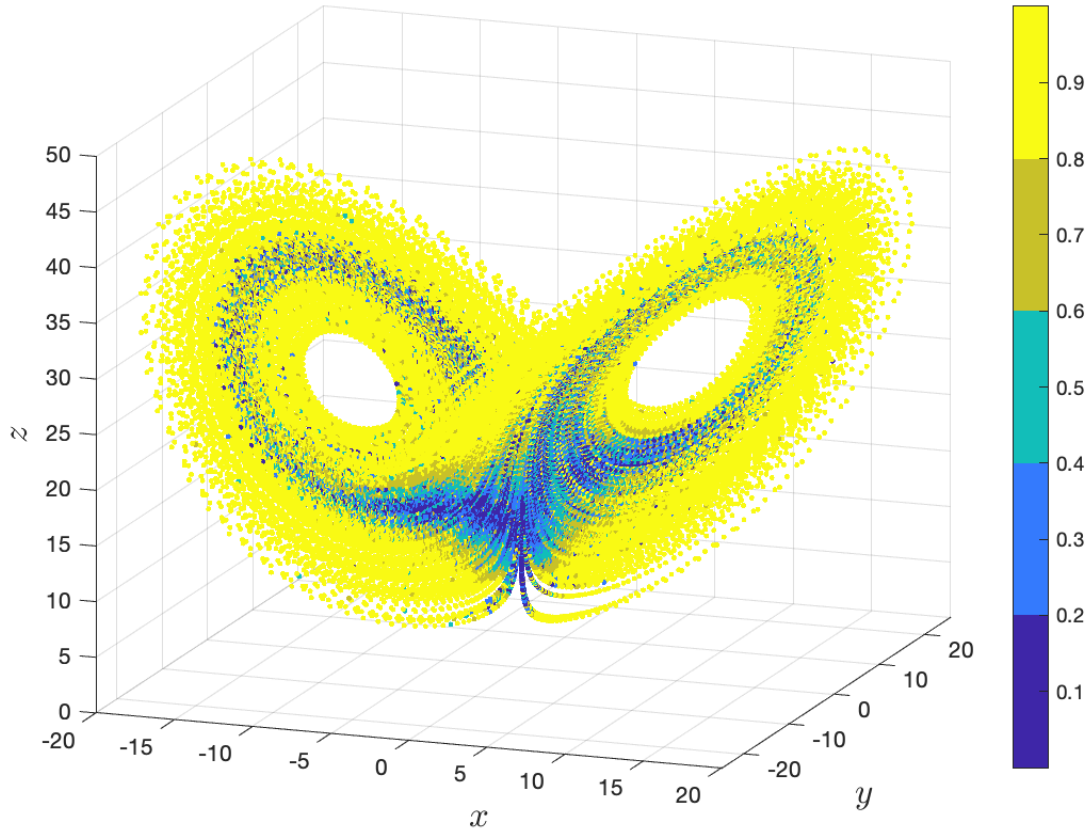


FIG. 6: Froyland’s algorithm on a simple Lorenz 63, $N = 100$, $\tau = 0.01$ (integration step).

The colors show the alignment θ_{12} , as defined in Eq. 2. Blue areas correspond to more stable areas, where the most unstable CLV and the near-neutral one are close to being orthogonal. Conversely, yellow areas are very unstable. This result proves robust under an increase of N , provided $N \geq 50$.

the method is tested with different values of m ranging from 1 to 5. For $m \leq 2$, the CLVs algorithm does not converge well on the FEM-BV-VAR reconstructed model. Thus we take $m = 3$, the smallest value for which the convergence is good enough. The higher m , the more complex the model can be (since the dimension of the auto-regressive model is $dim \times m$). With $m \leq 2$, the model may be too simple and may not capture the oscillatory patterns of the original system. Hence, the final choice is

$$K = 2, m = 3, p = 29,$$

454 where p is chosen thanks to the L-curve method. Fig. 7 shows an extract of the time series

455 of the original data (in yellow), the reconstructed model (in red) and the states affiliation
 456 found by the FEM-BV-VAR clustering (background in blue). Note that the neutral direction
 457 almost exists in the Lorenz system and leads to the oscillating dynamics. However, the FEM-
 458 BV-VAR reconstruction in Fig. 7 shows that the oscillations within a state are lost. This is a
 459 sign that the fitted AR model loses the near-neutral direction: an insight that is important
 460 for the following CLV analysis.

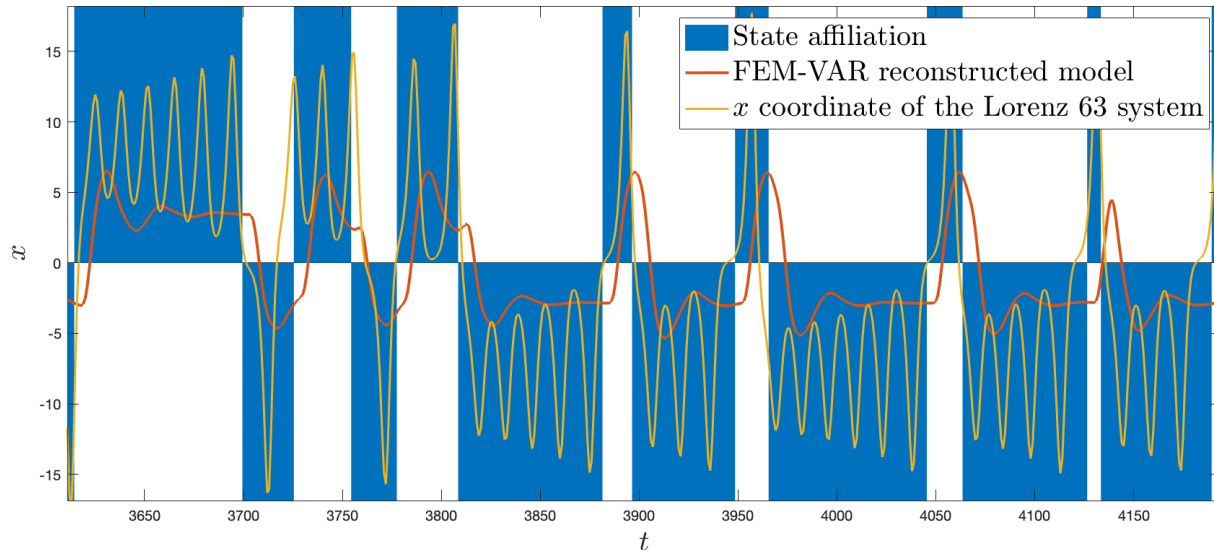


FIG. 7: FEM-BV-VAR clustering applied to a Lorenz 63. First component of the Lorenz
 system (yellow), states affiliation (blue and white strips) and reconstruction by the
 FEM-BV-VAR (red). For $K = 2$, $m = 3$, $p = 29$.

461 The next step is to choose $N = M$ (the number of push backward and push forward
 462 steps) and n (the correction steps) to run the CLVs algorithms (see Section II B). It turns
 463 out that the obtained result depends highly on this choice, as for the Von Kármán flow data,
 464 except that for the Lorenz system the range of validity of the method is much narrower.
 465 For intermediate values, such as $N = 10$ and $n = 5$, one can get some information on the
 466 attractor thanks to the alignment θ_{12} obtained through the FEM-BV-VAR approach. Fig. 8
 467 provides a picture that can be compared with the expected result from Fig. 6. The absolute
 468 values of θ_{12} along the trajectories are not the same as expected. However, one can see that
 469 the outbound of the wings is found to be less stable than the bulk. Hence, the method
 470 provides again an insight on the dynamics which is, however, less precise and accurate than
 471 in the two previous examples.

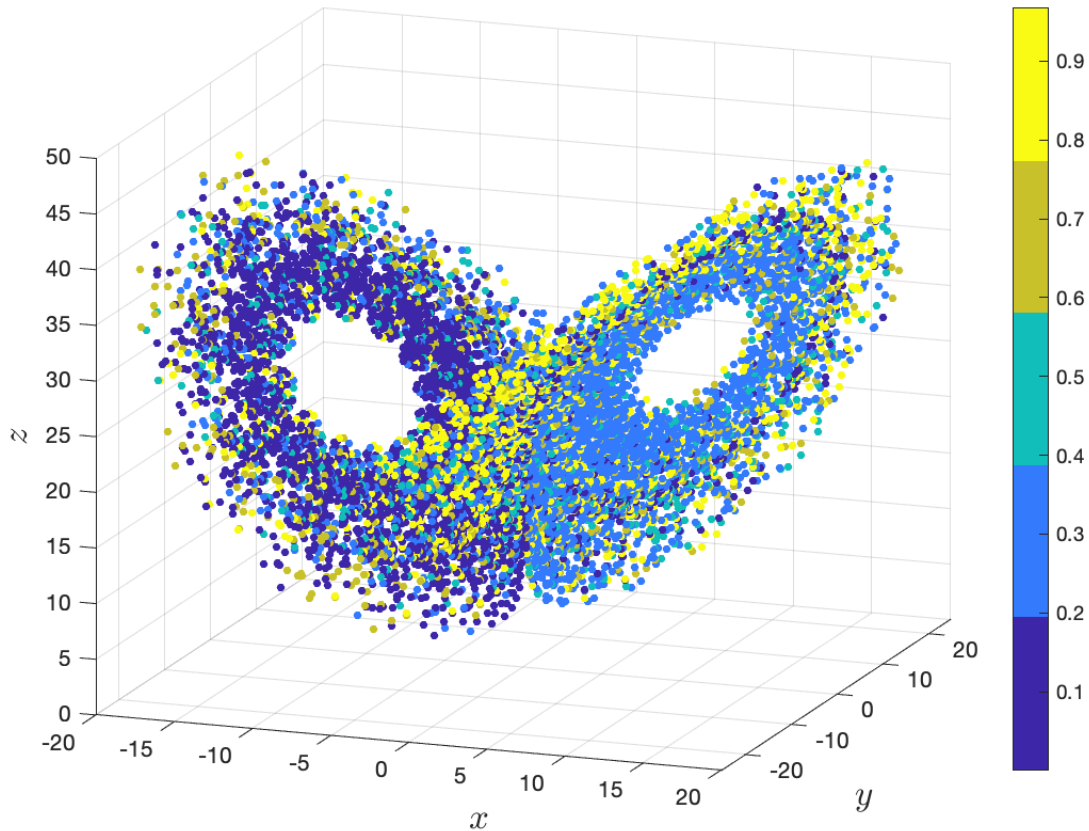


FIG. 8: Alignment of CLVs on a Lorenz 63 system, obtained thanks to the FEM-BV-VAR model. In color: θ_{12} . One can see that the outbound of the wings is found to be less stable than the bulk. CLVs computed with the Froyland algorithm ($N = 10$, $n = 5$), from the FEM-BV-VAR reconstruction with $K = 2$, $m = 3$, $p = 29$.

472 To evaluate the range of validity of the method, the same picture is generated for N
 473 ranging from 3 to 100 and n from 1 to 100. Two criteria are used to assess the relevance of
 474 the obtained result. First, given that the distribution of the value θ_{12} has to be the same in
 475 each wing (the two wings are dynamically symmetric), the average of θ_{12} is expected to be
 476 the same in each wing. To monitor that, one can look at the difference between the average
 477 value of θ_{12} over the two wings:

$$\Delta_{Lorenz} = \text{average of } \theta_{12} \text{ over the left wing} - \text{average of } \theta_{12} \text{ over the right wing} \quad (12)$$

478 Secondly, to have an indicator of noisiness of the obtained time series for θ_{12} , one can look
 479 at the total variation

$$TV = \sum_i |\theta_{12}(i+1) - \theta_{12}(i)| \quad (13)$$

480 The previously shown Fig. 8 was chosen to be the configuration that minimizes the total
 481 variation, keeping it strictly positive.

482 Fig. 9 shows, for each choice of (N, n) , the value of the difference Δ_{Lorenz} between the
 483 average alignment θ_{12} over the left wing and over the right one. This value is expected to be
 484 as close as possible to zero. One can see that for small values of N and n , the output is very
 485 asymmetric (blue zone in the bottom left), as well as for large values of N (red strip on the
 486 top). As previously explained, such an asymmetry is not physically relevant. Moreover, the
 487 total variation (Eq. (13)) tends to increase as N and n increase. Thus, unlike for the von
 488 Kármán flow data, the range of validity of this method in the N - n plane is small, making
 489 this method hardly usable in practice for the Lorenz system. While one can have some
 490 systematic methods to tune the FEM-BV-VAR parameters (K , m and p , see Section III B),
 491 no such tools exist to choose N and n .

492 This observation supports our key finding: the procedure does not work well when the
 493 system has no clear time-scale separation and when the FEM-BV-VAR reconstruction does
 494 not preserve the existence of an invariant neutral direction. As mentioned above, one can
 495 see in Figure 7 that the FEM-BV-VAR reconstructed model (in red) does not exhibit the
 496 oscillations within the wings that are characteristic of the original model (in yellow). Yet,
 497 those oscillations are important to capture the dynamics and predict the transition from
 498 one wing to the other, as suggested by Lorenz in his original paper³⁷. In fact, the FEM-BV-
 499 VAR model seems not be able to preserve the existence of a neutral direction (of which the
 500 oscillatory dynamics are a characteristic feature). Figure 10 shows the alignment θ (that
 501 is to say the cosine of the angle) between the tangent to the trajectory and the expected
 502 near-neutral CLV (as there are only three dimensions, the near-neutral CLV is the second
 503 one in this case). On the left, this alignment is computed for the Lorenz 63 system directly
 504 from the analytical expression. One clearly sees that almost everywhere the second CLV
 505 and the flow are aligned, which confirms the existence of a neutral direction in this system.
 506 However, the same computation but with the CLVs computed through the FEM-BV-VAR
 507 model shows different results. The picture is completely erratic, which means that the
 508 neutral direction is (almost) entirely lost. In summary the FEM-BV-VAR model fails to

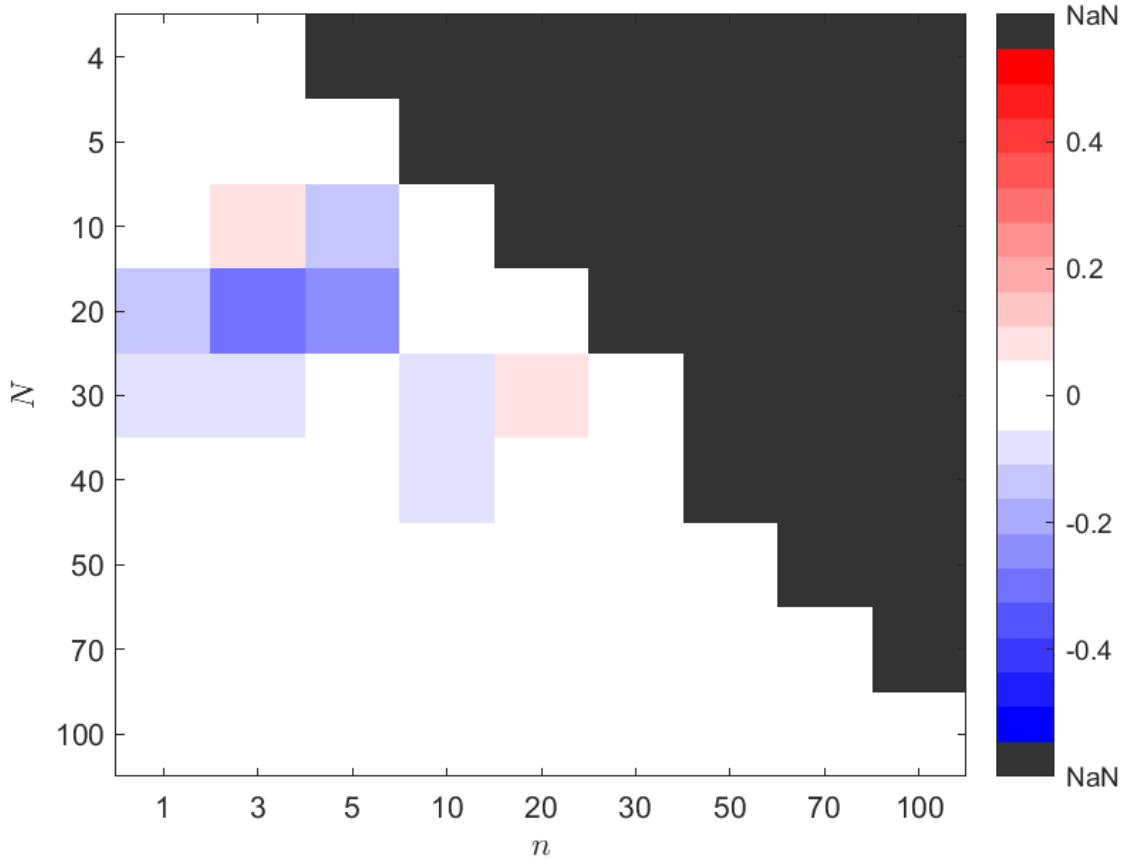


FIG. 9: Pcolor plot of Δ_{Lorenz} , the difference between the average value of θ_{12} over the two wings (see Eq. 12). N is in ordinate and n in abscissa. As the two wings are symmetric, in theory this difference should be close to zero (white area). One can see that for N and n not large enough, Δ_{Lorenz} can be far from zero, which means that the method does not converge well with this values.

509 capture the irregular oscillations of the system within each wing associated with such near-
 510 neutral directions. This is most likely related to the simple, linear model structure assumed
 511 in the FEM-BV-VAR approach.

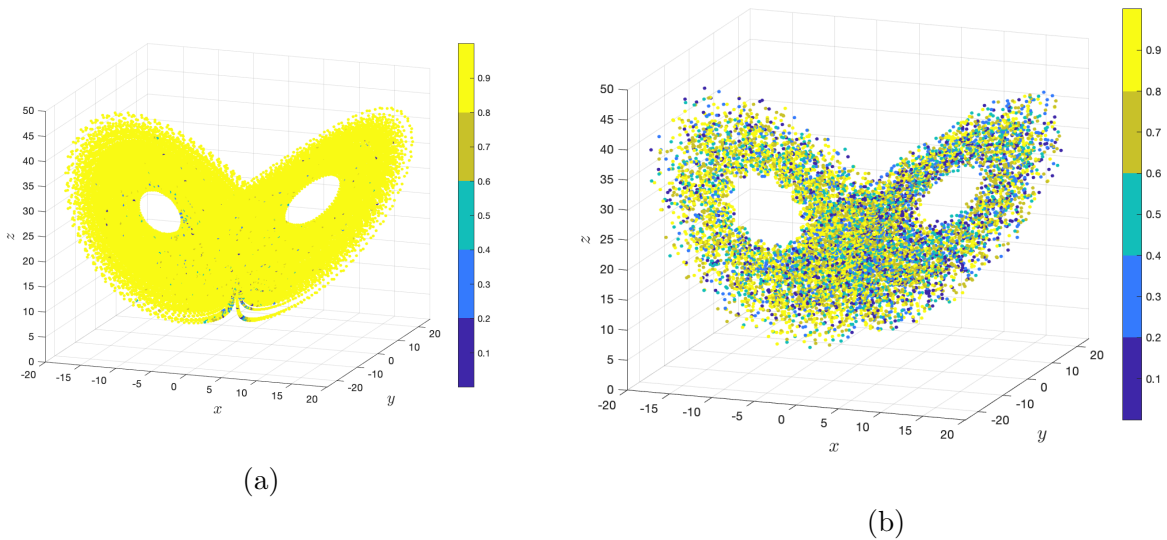


FIG. 10: (a) Alignment θ between the flow (tangent to the trajectory in each point) and the near neutral CLV, directly computed on a Lorenz system. Yellow corresponds to closely aligned vectors. (b) Same angle, but this time with the near neutral CLV computed on the FEM-BV-VAR reconstructed model. One can clearly see that in the first case, the near neutral CLV does correspond to the direction of the flow. However with the FEM-BV-VAR reconstruction, one completely loses this alignment.

512 **V. CONCLUSION**

513 The method described in this paper and suggested in earlier work by Quinn et al.¹³ makes
 514 it possible to compute an approximation of the Covariant Lyapunov Vectors (CLVs) from
 515 data series. It is based on the FEM-BV-VAR clustering scheme, which provides piece-wise
 516 auto-regressive linear models for the data. This model being built, one can compute an
 517 approximation of the CLVs. Under some conditions, the procedure seems to capture enough
 518 information on the dynamics to be able to give us the relative stability of the different areas
 519 of the phase space (that is to say, in this framework, the stability of the trajectory within
 520 each of the FEM-BV-VAR cluster). Information about stability of the trajectory is given
 521 by the analysis of the alignment between the most unstable (finite time) Lyapunov vector
 522 and the nearly neutral one (denoted θ_{12}).

523 We claim that this procedure works well provided the studied system exhibits two prop-

524 erties. First, it should have a clear scale separation in time, that is to say one should be able
525 to distinguish a temporal scale gap between two (or more) phenomena in the dynamics, as,
526 for instance, in standard fast-slow systems.

527 Secondly, the system has to support a dynamically invariant neutral direction in its
528 linearization and, importantly, this neutral direction has to be preserved as much as possible
529 by the FEM-BV-VAR reconstructed model. To support this hypothesis, we have tested the
530 validity of the method on three different systems with an increasing dynamical complexity:
531 the fast-slow FitzHugh-Nagumo oscillator, an embedded attractor built from von Kármán
532 flow data that exhibits a periodic orbit along with an saddle point, and finally a classic
533 Lorenz 63 chaotic attractor.

534 In the case of the FitzHugh-Nagumo oscillator, the method yields good performances: one
535 can find transitions precisely via the pattern of θ_{12} , as the method clearly identifies switches
536 between slow metastable regimes via unstable fast dynamics. This system exhibits a clear
537 time-scale separation that makes it possible for the FEM-BV-VAR model to capture most
538 of the relevant dynamical information, and especially to preserve the neutral direction. The
539 case of the von Kármán flow shows that the method can be relevant even with experimental
540 data, provided the dynamics exhibits a clear scale separation that allows the FEM-BV-VAR
541 to preserve the existence of a neutral direction in the reconstructed model. It also indicates
542 that one should be careful when tuning the values of N , M and n : they must be large
543 enough for Froyland’s algorithm to converge, but not too large to avoid the accumulation of
544 numerical errors. Finally, the Lorenz 63 example shows that for a system without a clear time
545 scale separation, the results are highly dependent on the hyper-parameters and therefore the
546 method is prone to fail. Due to its simple, linear model structure, the FEM-BV-VAR cannot
547 capture irregular, complicated short term dynamical patterns (as the oscillation around the
548 wing centers), and the reconstructed model does not show any direction that can be seen as
549 (near-)neutral.

550 Note that, while the reference approach by Quinn et al.¹³ assumes VAR models within
551 clusters, the clustering framework introduced by Horenko¹⁶ is general and can accommodate
552 more flexible model structures. Some alternative examples using different model structures
553 can be found in Metzner et al.¹⁷ and in de Wiljes et al.³⁸. In particular, Boyko et al.³⁹
554 recently extended this model-based clustering approach to enable the use of continuous
555 models, effectively fitting a nonstationary, nonlinear stochastic differential equation (SDE)

556 to timeseries of observations. Hence the data-driven computations of the CLVs could be
557 extended to using such a SDE-based clustering for the required model fitting step. Such
558 a future extension, based on a likely more faithful representation of complex multiscale
559 dynamics, may lead to more accurate estimation of the CLVs and hence to a better approach
560 to study transitions in complex systems such as the climate system.

561 ACKNOWLEDGMENTS

562 The authors thank the Ecole Normale Supérieure (ENS) for financial support enabling a
563 research exchange of AV during which this work was started. The authors acknowledge B
564 Dubrulle, F Daviaud and B Saint-Michel for granting the use of the von Kármán data. The
565 work benefited from discussions with Peter Koltai. M.E. has been supported by Germany’s
566 Excellence Strategy – The Berlin Mathematics Research Center MATH+ (EXC-2046/1,
567 project ID: 390685689).

568 DATA AVAILABILITY

569 The data that support the findings of this study are available from the corresponding
570 author upon reasonable request.

571 REFERENCES

- 572 ¹A. Katok and B. Hasselblatt, *Introduction to the modern theory of dynamical systems*, 54
573 (Cambridge university press, 1997).
- 574 ²P. Manneville, *Instabilities, chaos and turbulence*, Vol. 1 (World Scientific, 2010).
- 575 ³D. Ruelle, “Sensitive dependence on initial condition and turbulent behavior of dynamical
576 systems,” *Annals of the New York Academy of Sciences* **316**, 408–416 (1979).
- 577 ⁴F. Ginelli, P. Poggi, A. Turchi, H. Chaté, R. Livi, and A. Politi, “Characterizing dynamics
578 with covariant lyapunov vectors,” *Physical review letters* **99**, 130601 (2007).
- 579 ⁵C. L. Wolfe and R. M. Samelson, “An efficient method for recovering lyapunov vectors
580 from singular vectors,” *Tellus A: Dynamic Meteorology and Oceanography* **59**, 355–366
581 (2007).

- 582 ⁶S. Gilmore, “Lyapunov exponents and temperature transitions in a warming australia,”
583 *Journal of Climate* **32**, 2969 – 2989 (2019).
- 584 ⁷F. Nazarimehr, S. Jafari, S. M. R. H. Golpayegani, and J. Sprott, “Can lyapunov expo-
585 nent predict critical transitions in biological systems?” *Nonlinear Dynamics* **88**, 1493–1500
586 (2017).
- 587 ⁸Z. Toth and E. Kalnay, “Ensemble forecasting at nmc: The generation of perturbations,”
588 *Bulletin of the american meteorological society* **74**, 2317–2330 (1993).
- 589 ⁹N. Sharafi, M. Timme, and S. Hallerberg, “Critical transitions and perturbation growth
590 directions,” *Physical Review E* **96**, 032220 (2017).
- 591 ¹⁰M. W. Beims and J. A. Gallas, “Alignment of lyapunov vectors: A quantitative criterion
592 to predict catastrophes?” *Scientific reports* **6**, 1–7 (2016).
- 593 ¹¹E. L. Brugnago, J. A. C. Gallas, and M. W. Beims, “Predicting regime changes and
594 durations in lorenz’s atmospheric convection model,” *Chaos: An Interdisciplinary Journal*
595 *of Nonlinear Science* **30**, 103109 (2020), <https://doi.org/10.1063/5.0013253>.
- 596 ¹²C. Quinn, T. J. O’Kane, and V. Kitsios, “Application of a local attractor dimension to
597 reduced space strongly coupled data assimilation for chaotic multiscale systems,” *Nonlinear*
598 *Processes in Geophysics* **27**, 51–74 (2020).
- 599 ¹³C. Quinn, D. Harries, and T. J. O. Kane, “Dynamical analysis of a reduced model for the
600 north atlantic oscillation,” *Journal of the Atmospheric Sciences* **78**, 1647 – 1671 (2021).
- 601 ¹⁴G. Froyland, T. Hüls, G. P. Morriss, and T. M. Watson, “Computing covariant Lyapunov
602 vectors, Oseledets vectors, and dichotomy projectors: a comparative numerical study,”
603 *Phys. D* **247**, 18–39 (2013).
- 604 ¹⁵C. Martin, N. Sharafi, and S. Hallerberg, “Estimating covariant lyapunov vectors from
605 data,” *Chaos: An Interdisciplinary Journal of Nonlinear Science* **32**, 033105 (2022).
- 606 ¹⁶I. Horenko, “On the identification of nonstationary factor models and their application to
607 atmospheric data analysis,” *Journal of the Atmospheric Sciences* **67**, 1559–1574 (2010).
- 608 ¹⁷P. Metzner, L. Putzig, and I. Horenko, “Analysis of persistent nonstationary time series
609 and applications,” *Communications in Applied Mathematics and Computational Science*
610 **7**, 175–229 (2012).
- 611 ¹⁸V. I. Oseledec, “A multiplicative ergodic theorem. Characteristic Ljapunov, exponents of
612 dynamical systems,” *Trudy Moskov. Mat. Obšč.* **19**, 179–210 (1968).

- 613 ¹⁹B. Deremble, F. D’Andrea, and M. Ghil, “Fixed points, stable manifolds, weather regimes,
614 and their predictability,” *Chaos: An Interdisciplinary Journal of Nonlinear Science* **19**,
615 043109 (2009).
- 616 ²⁰J. A. Hartigan and M. A. Wong, “Algorithm AS 136: A K-Means Clustering Algorithm,”
617 *Journal of the Royal Statistical Society. Series C (Applied Statistics)* **28**, 100–108 (1979),
618 publisher: [Wiley, Royal Statistical Society].
- 619 ²¹L. Rabiner, English “A Tutorial on Hidden Markov-Models and Selected Applications in
620 Speech Recognition,” *Proceedings of the Ieee* **77**, 257–286 (1989).
- 621 ²²N. Vercauteren and R. Klein, “A Clustering Method to Characterize Intermittent Bursts of
622 Turbulence and Interaction with Submesoscale Motions in the Stable Boundary Layer,” *Journal*
623 *of Atmospheric Sciences* **72**, 1504–1517 (2015).
- 624 ²³V. Boyko and N. Vercauteren, “Multiscale Shear Forcing of Turbulence in the Nocturnal
625 Boundary Layer: A Statistical Analysis,” *Boundary-Layer Meteorology* **179**, 43–72 (2021),
626 publisher: Springer Netherlands.
- 627 ²⁴T. J. O’Kane, J. S. Risbey, C. Franzke, I. Horenko, and D. P. Monselesan, “Changes
628 in the metastability of the midlatitude southern hemisphere circulation and the utility of
629 nonstationary cluster analysis and split-flow blocking indices as diagnostic tools,” *Journal*
630 *of the atmospheric sciences* **70**, 824–842 (2013).
- 631 ²⁵T. J. O’Kane, R. J. Matear, M. A. Chamberlain, J. S. Risbey, B. M. Sloyan, and
632 I. Horenko, en “Decadal variability in an OGCM Southern Ocean: Intrinsic modes, forced
633 modes and metastable states,” *Ocean Modelling* **69**, 1–21 (2013).
- 634 ²⁶C. Rödenbeck, C. Beck, and H. Kantz, “Dynamical systems with time scale separation:
635 averaging, stochastic modelling, and central limit theorems,” in *Stochastic Climate Models*
636 (Springer, 2001) pp. 189–209.
- 637 ²⁷J. Wouters and V. Lucarini, “Multi-level dynamical systems: Connecting the ruelle re-
638 sponse theory and the mori-zwanzig approach,” *Journal of Statistical Physics* **151**, 850–860
639 (2013).
- 640 ²⁸S. Shoffner and S. Schnell, “Approaches for the estimation of timescales in nonlinear dy-
641 namical systems: Timescale separation in enzyme kinetics as a case study,” *Mathematical*
642 *biosciences* **287**, 122–129 (2017).
- 643 ²⁹T. Alberti, D. Faranda, R. V. Donner, T. Caby, V. Carbone, G. Consolini, B. Dubrulle,
644 and S. Vaienti, “Small-scale induced large-scale transitions in solar wind magnetic field,”

645 The Astrophysical journal letters **914**, L6 (2021).

646 ³⁰R. FitzHugh, “Mathematical models of threshold phenomena in the nerve membrane,”
647 Bull. Math. Biophysics **17** (1955).

648 ³¹N. Fenichel, “Geometric singular perturbation theory for ordinary differential equations,”
649 J. Differential Equations **31**, 53–98 (1979).

650 ³²C. Kuehn, *Multiple time scale dynamics*, Applied Mathematical Sciences, Vol. 191
651 (Springer, Cham, 2015) pp. xiv+814.

652 ³³P.-P. Cortet, A. Chiffaudel, F. Daviaud, and B. Dubrulle, “Experimental evidence of a
653 phase transition in a closed turbulent flow,” Physical review letters **105**, 214501 (2010).

654 ³⁴B. Saint-Michel, F. Daviaud, and B. Dubrulle, “A zero-mode mechanism for spontaneous
655 symmetry breaking in a turbulent von kármán flow,” New Journal of Physics **16**, 013055
656 (2014).

657 ³⁵D. Faranda, Y. Sato, B. Saint-Michel, C. Wiertel, V. Padilla, B. Dubrulle, and F. Daviaud,
658 “Stochastic chaos in a turbulent swirling flow,” Phys. Rev. Lett. **119**, 014502 (2017).

659 ³⁶B. Dubrulle, F. Daviaud, D. Faranda, L. Marié, and B. Saint-Michel, “How many modes
660 are needed to predict climate bifurcations? lessons from an experiment,” Nonlinear Pro-
661 cesses in Geophysics **29**, 17–35 (2022).

662 ³⁷E. N. Lorenz, “Deterministic nonperiodic flow,” Journal of atmospheric sciences **20**, 130–
663 141 (1963).

664 ³⁸J. de Wiljes, A. J. Majda, and I. Horenko, English “An adaptive Markov chain Monte
665 Carlo approach to time series clustering of processes with regime transition behavior,”
666 Multiscale modeling & simulation **11**, 415–441 (2013).

667 ³⁹V. Boyko, S. Krumscheid, and N. Vercauteren, “Statistical learning of non-linear stochas-
668 tic differential equations from non-stationary time-series using variational clustering,”
669 arXiv:2102.12395 [math] (2021), arXiv: 2102.12395.